Sl. No.	IIT Ropar List of Recent Publications with Abstract Coverage: August, 2022
1.	3D-DSPnet: Product Disassembly Sequence Planning A Upadhyay, B Ladrecha, A Dubey, SM Kuriakose, P Goenka - IEEE International Conference on Multimedia and Expo Workshops (ICMEW), 2022 **Abstract:** Product Disassembly has become an area of active research as it supports sustainable development by aiding effective end-of-life (EOL) stage strategies like reuse, re-manufacturing, recycling, etc. In this work, we propose a new approach, 3D-DSPNet, that can utilize 3D data from CAD assembly models to generate a feasible disassembly sequence. Our approach uses Graph-based learning to process the graph representation of CAD models. Currently, the available 3D CAD model datasets lack ground truth disassembly sequences. We propose and curate a new dataset, the 3D-DSP dataset, which includes ground truth information about the disassembly sequence for 3D product models. We carry out evaluation and analysis of results to explain the efficacy of the proposed method. Our approach significantly outperforms the existing baseline. We develop an Autodesk Fusion 360 plug-in that generates disassembly sequence animation, allowing intuitive analysis of the disassembly plan.
2.	A deep learning multi-layer perceptron and remote sensing approach for soil health based crop yield estimation A Tripathi, RK Tiwari, SP Tiwari - International Journal of Applied Earth Observation and Geoinformation, 2022 **Abstract:** In recent years, Deep Learning Multi-Layer Perceptron (DLMLP) neural networks have shown remarkable success in addressing crop yield forecast related problems. The methodologies used so far for crop yield forecast with remotely sensed data were focused upon vegetation indices generated from optical data. The prediction of crop yield in an accurate manner by developing robust machine learning models based on soil health parameters is crucial since it helps keep a track of soil health as well as its impact on overall yield. This study aims to utilize remotely sensed Microwave satellite data from Sentinel-1 and optical data from Sentinel-2, and field data to estimate three important soil health parameters- Soil Moisture, Soil Salinity, and Soil Organic Carbon (SOC). The study has been carried out in the Rupnagar district of Punjab in India. The estimated soil health parameters, SAR backscatter, and optical remote sensing satellite data parameters were utilized to estimate wheat crop yield. The soil health based DLMLP model performed best in crop yield estimation and gave R^2 values of 0.723 and 0.684 in the training and testing phases, respectively, and Mean Absolute Error (MAE) of 0.98 and Root Mean Square Error (RMSE) value of 1.24 for the 2019–20 season. The DLMLP test R^2 was 42.2% more than the Ordinary Least Squares Regressor (OLS), while the MAE and RMSE were 37.97% and 38.61% less than the OLS regressor for wheat crop yield estimation. The soil health-based DLMLP model gave satisfactory yield estimation accuracy in the absence of validation of soil health parameter values for the preceding years-2015–16 till 2018–19 wheat seasons. This study's novel feature is that it estimates soil health parameters for the early stages of wheat crop growth when soil lies mostly exposed and utilises them for crop yield prediction. **Graphical Abstract:**

	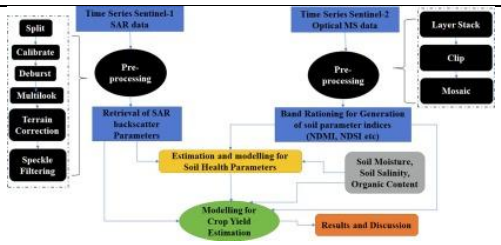
3.	A Novel Multigain Single-Stage Grid-Connected Inverter With Asynchronous Switching for Intra-Inverter Circulating Current Elimination BK Gupta, KR Sekhar, A Kumar - IEEE Transactions on Power Electronics, 2022 **Abstract:** At present, the single stage inverters are popular in integrating large-scale solar farms with distribution networks that demand higher dc bus voltage. The elevated dc potentials would degrade the reliability of the solar panels and inverter modules. In this work, the multiboost solar inverter topologies of three variants are presented for grid-connected applications. Since the proposed topologies aim to achieve higher voltage boost at ac side with reduced dc bus potential, it is required to use asynchronous switching strategies, unlike parallel inverter configurations. Although the proposed topologies are advantageous in-terms of improved reliability of solar panels and inverter modules, but instantaneous characteristic impedance imbalance due to asynchronous switching provokes circulating current within the inverter modules. Since the circulating current is undesirable concerning power quality and thermal aspects, in this work, the method of instantaneous impedance balance is ensured with the specially designed switching algorithm for proposed topologies. The eliminated instantaneous circulating current provides the flexibility of operating all inverter modules with the common dc bus. The proposed high gain boost configurations and switching methodologies are demonstrated on hardware prototype by pumping 2.4-kW power to the grid.
4.	A Planar Switching Integrated Quadrant Coil Antenna to form Widespread Switched Polarized H-field for Misalignment Resilient WPT System VK Srivastava, A Sharma - IEEE Transactions on Antennas and Propagation, 2022 **Abstract:** This paper presents a planar switching integrated quadrant coil antenna to mitigate lateral and angular misalignment problems in near-field wireless power transfer (WPT) applications. To allow a completely free receiver movement, both the misalignment problems are concurrently addressed by forming widespread distributions of switched polarized H-field in the receiver region. To achieve this, current circulations through the four quadrant coils composing the proposed antenna are judiciously controlled to form three orthogonal H-field components. For lateral misalignment mitigation, the widespread field distributions are obtained by using a field-forming approach for optimizing the antenna parameters. To produce the switched polarized H-field for angular misalignment mitigation, time-switching of the orthogonal H-field components is performed. This switching operation is realized by three DPDT switches inter-connecting the coils and integrated within the design for a cost-effective planar antenna solution. The fabricated prototype is measured and the experimental results are corroborated with the analysis. The results demonstrate potential of the proposed antenna to simultaneously mitigate both the misalignment problems for medium-range WPT of small devices which are allowed to freely rotate and displace such as medical implants, wireless endoscopy capsules and wearable devices etc.

5.	[A strategic review on gallium oxide based power electronics: Recent progress and future prospects] S Dahiya, D Kaur, A Ghosh, M Kumar - Materials Today Communications, 2022 **Abstract:** Silicon based power devices have limited capabilities in terms of voltage handling and switching speeds, leading to rampant research in the field of next generation wide bandgap semiconductors like SiC, GaN, and Ga_2O_3. Amongst these, gallium oxide with its ultra-wide bandgap of 4.6–4.9 eV and high breakdown field (approx. 8 MV cm^{-1}) turns out to be a potential replacement. Availability of large size, high-quality wafers at moderate costs make it desirable even from industrial viewpoint. Ga_2O_3 power diodes having breakdown voltages (V_{br}) of hundreds of Volts have been reported. However, they suffer from very high on-resistance (R_{on}) leading to increased switching losses and decreased switching speed. This timely review analyses the recent progress made in Ga_2O_3 based power devices with detailed discussion on the basic parameters such as V_{br}, R_{on} and leakage current along with the factors critically affecting them. Special focus is laid on the impeccable value-additive extreme environment applications. Open challenges plaguing the field such as trade-off between achieving high V_{br} and low R_{on} simultaneously, shortcomings in the material itself and the need for new physics to explain the high energy carrier transport is also explored along with the future prospects required to achieve true power-saving and commercialization. **Graphical Abstract:** 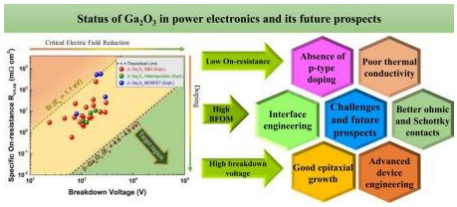
6.	[A Switched Planar Multi-Coil Transmitter Antenna Designed with Non-uniform H-field Forming for Small Device Localization] A Sharma, VK Srivastava - IEEE Transactions on Antennas and Propagation, 2022 **Abstract:** To monitor 3-D position and orientation of a small device having planar receiver coil, a switched multi-coil transmitter antenna is proposed by adopting time-divisional approach. The existing multi-frequency methods require eight or more input ports to feed the coils with multi-frequency signals for localization. In contrast, the proposed transmitter antenna is driven by a single frequency source and uses only three input ports for reduced complexity. Moreover, the multiple coils of the proposed antenna are optimally grouped to form non-uniform magnetic-field distribution using three switches in such a manner that better localization accuracy is achieved as compared to the multi-frequency design. Rigorous analysis and simulations are performed to investigate the performance of the proposed design and localization approach. To validate the claim, experimental study results proved the potential of the proposed antenna employed for tracking a planar receiver in applications like medical robots, navigation of blind people, virtual reality, etc.
7.	[A Variational Principle Based Approach for General Solution to Transverse Isotropic Axisymmetric Cylinder Problem] A Sirsat, SS Padhee - Journal of Applied Mechanics, 2022

	Abstract: Deformation of solid or hollow cylinders with transverse isotropic material under axisymmetric loading is one of the oldest problem. A general field solution is highly sought after, as this problem finds application in various fields. In the present work this problem has been formulated starting with basic curvilinear kinematics and governing equations are derived using Reissner's variational principle. Non-singular solutions have been derived and have been validated with literature for specific cases.
8.	An active inductor employed CML latch for high speed integrated circuits P Singh, MK Singh, VG Hande, M Sakare - Analog Integrated Circuits and Signal Processing, 2022 **Abstract:** This paper proposes an inductor-less D-latch. In the proposed D-latch, negative feedback is used that makes input impedance appears to be inductive for the high-frequency input signal. The bandwidth is increased by around 23% due to this effect. Two applications are shown in this paper to verify the proposed latch operation: a pseudo-random binary sequence (PRBS) generator and a serializer. The speed of the PRBS generator and serializer has improved by 15.8% and 23% using the proposed latch, respectively. The post-layout simulation results in 90 nm CMOS technology with a power supply of 1 V prove the concept. To study functional correctness and scalability of the proposed architecture to lower technology nodes, 22 nm PTM model is used and verified the correct operation of the proposed architecture.
9.	Analysis of Buckley-Leverett Problem for Water Flooding in Oil Reservoir Rock: Analytical and Numerical Modeling Z Hafsi, L Ayed, M Mishra, S Elaoud - International Conference Design and Modeling of Mechanical Systems, Design and Modeling of Mechanical Systems - V, 2022 **Abstract:** The Buckley-Leverett (BL) displacement theory gives a simplified formulation of governing equations controlling oil-water flow in an oil reservoir rock. Formulated under some specific hypothesis, the BL problem has the advantages of being analytically solvable for invading fluid saturation. This paper sheds the light on the Buckley-Leverett problem through analytical and numerical resolutions. An overview on basic mathematical formulations was presented. Then a 1D example was detailed in order to plot the saturation profile of the wetting phase by combining the analytical solution of the front equation with the Welge construction method. Additionally a COMSOL Multiphysics model was built and both numerical and analytical results were compared. Furthermore, the numerical model was extended for a 2D example and obtained wetting saturation profiles plotted along the length of the domain were compared with previous literature outcomes. Two different modules of COMSOL Multiphysics were used to build numerical models. The 1D model reposes on the coefficient form PDE module that permits writing governing equations under matrix form and then solving for the unknown saturation. For the 2D model the capability of COMSOL Multiphysics in coupling different modules has served to implement the model through using both modules viz. phase transport in porous media and Darcy’s law.
10.	Analysis of differential glacier behaviour in Sikkim Himalayas in view of changing climate S Guha, RK Tiwari - Geocarto International, 2022 **Abstract:** The assessment of temporal changes in glacier response due to climatic change is critical from the hydrological perspective. The present study aims to identify temporal changes in

	glacier response using area changes, retreat, and surface elevation changes. The Friedman test and Wilcoxon signed-rank test were introduced to identify the temporal changes in the parameters mentioned above for the entire Sikkim from a sample of 28 studied glaciers. The result shows the area changes lies between 0.044–0.462, 0.143–0.351, 0.083–0.685, and 0.157–1.39%y^{-1} between 1988–2000, 2000–08, 2008–14 and 2014–18, respectively. Further, the magnitude of deglaciation has increased after 2014 by 73%, 76%, and 100% compared to the third, second, and first timeframe. Likewise, retreat is 10.82 ± 3.53, $19.07 \pm 4.19, 13.32 \pm 5.59, 23.44 \pm 5.3$ my^{-1} between 1998–2000, 2000–08, 2008–14 and 2014–18, respectively in the sample glaciers. Additionally, surface elevation change shows a negative-accelerated trend in the sample glaciers from 0.15 to 1.92 my^{-1} to 0.88 to 2.52 my^{-1} between 2000–08 and 2008–18, respectively.
11.	Analysis of Drone Assisted Network Coded Cooperation for LoS Environments P Kumar, S Darshi, S Shailendra - Wireless Personal Communications, 2022 **Abstract:** This paper consider a Drone Assisted Network Coded Cooperation (DA-NCC) scenario for Line of Sight (LoS) channel environments. For analysing the performance of DA-NCC, Decode-and-Forward (DF) protocol is used at the drone and Selection Combining (SC) is performed at the destination node. An analytical closed-form formulation of the outage probability is devised and proven through simulations to assess network performance of the DA-NCC system. In order to have a better understanding of deterministic networks, a discussion on capacity and a comparison of alternative rectangular designs for deterministic networks are also presented. Insightful results on the relation among drone height, DNC-noise and network geometry may play an important role during the performance analysis of the DA-NCC system. Using closed-form expressions of performance measures, system designers can quickly examine the effects of various parameters on the DA-NCC network's performance.
12.	Anomaly Detection in Audio with Concept Drift using Dynamic Huffman Coding P Kumari, M Saini - IEEE Sensors Journal, 2022 **Abstract:** When detecting anomalies in audio, it can often be necessary to consider concept drift: the distribution of the data may drift over time because of dynamically changing environments, and anomalies may become normal as time elapses. We propose to use dynamic Huffman coding for anomaly detection in audio with concept drift. Compared with the existing method of adaptive Gaussian mixture modeling (AGMM), dynamic Huffman coding does not require a priori information about the clusters and can adjust the number of clusters dynamically depending on the amount of variation in the audio. To control the size of the Huffman tree, we propose to merge clusters that are close to each other instead of replacing rare clusters with new data. This reduces redundancy in the Huffman tree while ensuring that it never forgets past information. On audio datasets with concept drift which we have curated ourselves, our proposed method achieves a higher area under the curve (AUC) compared with AGMM and fixed-length Huffman trees.
13.	Artificial intelligence uncovers carcinogenic human metabolites A Mittal, SK Mohanty, V Gautam, S Arora, ..S Saproo, R Gupta, ..S Naidu.. - Nature Chemical Biology, 2022 **Abstract:** The genome of a eukaryotic cell is often vulnerable to both intrinsic and extrinsic threats owing to its constant exposure to a myriad of heterogeneous compounds. Despite the

	availability of innate DNA damage responses, some genomic lesions trigger malignant transformation of cells. Accurate prediction of carcinogens is an ever-challenging task owing to the limited information about bona fide (non-)carcinogens. We developed Metabokiller, an ensemble classifier that accurately recognizes carcinogens by quantitatively assessing their electrophilicity, their potential to induce proliferation, oxidative stress, genomic instability, epigenome alterations, and anti-apoptotic response. Concomitant with the carcinogenicity prediction, Metabokiller is fully interpretable and outperforms existing best-practice methods for carcinogenicity prediction. Metabokiller unraveled potential carcinogenic human metabolites. To cross-validate Metabokiller predictions, we performed multiple functional assays using Saccharomyces cerevisiae and human cells with two Metabokiller-flagged human metabolites, namely 4-nitrocatechol and 3,4-dihydroxyphenylacetic acid, and observed high synergy between Metabokiller predictions and experimental validations.
14.	Autofocused asymmetric aberration laser beams S Singh, V Dev, V Pal - International Conference Laser Optics (ICLO), 2022 **Abstract:** We have generated asymmetric aberration laser beams (aALBs) with auto-focusing properties. The asymmetry in the phase distribution of aALBs is deliberately exploited for controlling spatial intensity distribution, and thereby generating high-power densities, useful for several applications.
15.	Bilayer graphene/HgCdTe heterojunction based novel GBn infrared detectors S Bansal, Avishek Das, K Prakash, N Sardana - Micro and Nanostructures, 2022 **Abstract:** This paper presents different configurations of bilayer graphene (BLG)/mercury cadmium telluride ($Hg_{1-x}Cd_xTe$) based GBn detectors operating in the mid- and long-wave infrared (IR) regime. One type of configuration consists of a contact graphene layer (G) of p^+-BLG and a barrier layer (B) of p^--$Hg_{1-x}Cd_{x=0.41}Te$ deposited on the n^+-$Hg_{1-x}Cd_xTe$ absorber layer (n) and is named as p^+-p^--n^+ detector. In another configuration, the n^+-BLG contact layer and n^--$Hg_{1-x}Cd_{x=0.41}Te$ barrier layer are deposited on n^+-$Hg_{1-x}Cd_xTe$ absorber layer and is called a n^+-n^--n^+ unipolar detector. The Silvaco Atlas TCAD software is used for the optoelectronic characterizations which closely matches the results obtained through analytical modeling. The proposed GBn detectors demonstrate about 10^6 times improvement in photocurrent density and self-powered mode operation. The proposed detectors demonstrate rapid photoswitching time <0.1 ps. The external quantum efficiency (QE_{ext}) of 26.06, 11.68, 54.08, and 50.53% are found for p^+-p^--n^+ mid-wave, p^+-p^--n^+ long-wave, n^+-n^--n^+ mid-wave, and n^+-n^--n^+ long-wave IR detectors, respectively, at −0.5 V and 77 K. Such detection performances are ascribed to the huge built-in electric field at contact/barrier heterojunction, and large barrier height in conduction band resulting in enhanced photogenerated carriers which contributes to the net photocurrent. Further, it is shown that the multiplication effect of carriers in BLG and high electric field across the interface results in the QE_{ext} >100% at near room temperature.
16.	Con-Net: A Consolidated Light-Weight Image Restoration Network N Mehta, S Murala - IEEE Transactions on Broadcasting, 2022 **Abstract:** There has been a considerable gap between the recent high-resolution display technologies and the short storage of its content. However, most of the existing restoration methods are restricted by local convolution operations and equal treatment of the diverse information in degraded image. These approaches being degradation-specific employ the same

	rigid spatial processing across different images ultimately resulting in high memory consumption. For overcoming this limitation we propose Con-Net, a network design capable of exploiting the non-uniformities of the degradations in spatial-domain with limited number of parameters (656k). Our proposed Con-Net comprises of basically two main components, (1) a spatial-degradation aware network for extracting the diverse information inherent in any degraded image, and (2) a holistic attention refinement network for exploiting the knowledge from the degradation aware network to selectively restore the degraded pixels. In a nutshell, our proposed method is generalizable for three applications: image denoising, super-resolution and real-world low-light enhancement. Extensive qualitative and quantitative comparison with prior arts on 8 benchmark datasets demonstrates the efficacy of our proposed Con-Net over existing state-of-the-art degradation-specific architectures, by huge parameter and FLOPs reduction in all the three tasks.
17.	Data-Driven Phase Selection, Property Prediction and Force-Field Development in Multi-Principal Element Alloys D Beniwal, PK Ray - Forcefields for Atomistic-Scale Simulations: Materials and Applications, Lecture Notes in Applied and Computational Mechanics, 2022 **Abstract:** Multi-Principal Element Alloys (MPEAs) have brought a paradigm shift in the alloy design process and pose a significant challenge due to the astronomical and compositional space available for exploration. Since experimental and ab-initio methods are more suitable for targeted alloy design over a narrow composition range, data-driven methodologies have shown promise in the search for alloys with unique or improved properties. This chapter introduces the field of materials informatics by laying out the fundamentals of machine learning, i.e., the types of problems, dataset formulation, feature selection, and machine learning algorithms, as applied to materials science. It follows with a holistic review of the existing data-driven models targeted towards the prediction of phase selection, mechanical properties and ordering behaviour in MPEAs. It also discusses the methodology for the development of machine learning force fields that enable atomistic modelling of various phenomena, such as diffusion, phase transformations and mechanical deformation, in MPEAs
18.	Design and synthesis of circular antenna array using artificial hummingbird optimization algorithm H Singh, S Singh, A Gupta, A Gehlot, J Kaur - Journal of Computational Electronics, 2022 **Abstract:** Circular antenna arrays are extensively utilized in next-generation communication applications like IoT, 5G, and beamforming, although maintaining the subsidiary lobes along with directivity remains a barrier. Many conventional methods might be employed to estimate the array parameters in real-time, but they would lag in maintaining high directivity and a low side lobe level. An optimization problem is used in this study to get the requisite primary lobe orientation, inhibit the subsidiary lobe and optimize directivity. To estimate the regulating parameters in a timely way, an artificial hummingbird method is employed for the circular antenna array issue. Simulations are run, and the results are compared to those of other standard techniques. The results reveal that the artificial hummingbird method achieves great side lobe reduction while maintaining acceptable directivity. According to the dimension study, high directivity values with low side lobe levels may be attained with fewer antenna parts as well.
19.	Development of entropy and deviation-based water quality index: Case of river Ganga, India M Verma, VA Loganathan, VK Bhatt - Ecological Indicators, 2022

	Abstract: In this study, a comprehensive multiplicative water quality index, M_{ED}-WQI, for surface water quality assessment has been developed that uses sub-index functions based on deviation from maximum contaminant level of respective parameters. The parametric weights in M_{ED}-WQI were computed using entropy based approach to eliminate subjectivity. Using a synthetic dataset the performance of M_{ED}-WQI has been compared with Composite WQI (CWQI) that is based on Saaty's analytical hierarchical process. The results indicated that in comparison to CWQI, M_{ED}-WQI approach provides an objective and rational framework that eliminates clustering effect in providing the water quality status. Further, M_{ED}-WQI has been applied to an exhaustive water quality dataset of river Ganga, one of the major perennial rivers of India. Out of 224 sampling locations, 167 sites have been associated with excellent or good water quality class whereas 57 sites are identified with either fair, poor, or heavily-polluted water quality class. Furthermore, the water quality classes correlated well with the type of anthropogenic activities carried out at the site.
20.	Discharge Pulse Analysis Based Machining Responses in Vibration Assisted µEDM Processes S Raza, R Nadda, CK Nirala - MAPAN, 2022 **Abstract:** The frequent occurrence of inherent abnormal discharges with the progress of machining in resistance–capacitance (RC) based micro-electrical discharge machining (µEDM) affects the product quality and material removal rate (MRR). This work presents a data acquisition-based analysis to address these alterations by exploring the nature of discharge pulses of vibration-assisted µEDM process variants. A cost-effective vibrating spindle attachment is developed for preliminary testing of vibration assistance to the controlled RC-based µEDM and reverse-µEDM processes. Micro-grooves of 5 mm ×× 500 µm ×× 500 µm and arrayed micro-rods with an aspect ratio of 20 with a diameter of 0.1 mm were fabricated using µED-milling and reverse-µEDM, respectively. Two different frequencies, 100 and 150 Hz, are used in vibration-assisted machining, leading to a maximum 57% reduction in machining time. The discharge pulses acquired during the machining showed a significant decrease in the arcing phenomenon that helps to understand the variation in MRR, surface finish, and overcut.
21.	Do Knowledge and Technology-Intensive Industries Spatially Concentrate in Rural and Urban Areas of India? Evidence from Economic Census Micro-Level Data S Agarwal, SR Behera - Theoretical Economics Letters, 2022 **Abstract:** This paper investigates the geographic concentration of knowledge and technology-intensive (KTI) industries, covering 0.43 million establishments across various districts of rural and urban areas in India. Using the spatially weighted Ellison-Glaeser index, cartogram and choropleth map results show that few KTI industries are highly geographically concentrated in urban and rural areas, specific to certain districts and a few Indian states. Within highly employable states of India, workers are employed in only a particular location of a few districts. Also, we differentiate between urban and rural concentrated and urban and rural dispersed districts within highly employable states. In addition, results validate the extent of the geographical concentration of KTI industries in rural and urban areas of highly employable Indian states. Further, results exhibit that industries spatially concentrate in only a few locations across specific districts in India, indicating natural advantages and other economic forces are pretty strong in certain areas. Besides, results suggest that the demand-based networks and push-and-pull supply chains are well established in a specific location of a few districts, incentivizing

	other firms to locate their business, which creates a spatial spillover effect and benefits all economic agents. Empirical results suggest that policymakers in India could unleash the resource potential of spatially concentrated districts by implementing a location-based policy and considering multi-level governance and informal and formal institutions, which could further boost regional economic growth.
22.	Do Neighbourhood Effects Matter for the Geographical Concentration? Evidence from the Indian Industries S Agarwal, SR Behera - Theoretical Economics Letters, 2022 **Abstract:** This paper investigates the impact of neighbouring effects on the geographical concentration of manufacturing and service industries at the district level using India's Economic Census (2013) data. As empirical literature suggests, spillovers do not recognize areal boundaries, and spatial dependence among regions needs to be incorporated while quantifying the geographical concentration of industries. In this context, we employ the spatially weighted Ellison-Glaeser (EG) index to evaluate the impact of neighbourhood effect on the spatial concentration of 71 manufacturing and 120 service industries in India. Using aggregate data at the district level by covering 636 districts and 34 states and union territories in India, empirical results exhibit that the magnitude of the neighbourhood effect does not substantially impact the geographical concentration of 191 industries. More specifically, the neighbourhood effect is over-shadowed while considering an aggregate of 636 districts covering all states and union territories in India. To gain more insight into the role of neighbourhood effects and for robustness checks, we measure manufacturing and service industries' geographical concentration within India's 29 contiguous states and union territories. Our subsequent empirical evidence validates that neighbourhood effects are well captured by the spatially weighted Ellison-Glaeser index for the top three highly concentrated manufacturing and service industries. Moreover, we find that the spatially weighted EG index plays a predominant role while computing geographical concentration for the highly concentrated manufacturing and service industries across various Indian states and union territories at the district level in India.
23.	Effect of micelle breaking rate and wall slip on unsteady motion past a sphere translating steadily in wormlike micellar solutions C Sasmal - Physics of Fluids, 2022 **Abstract:** Many prior experimental studies have found the existence of an unsteady or fluctuating flow field around a solid sphere when falling in wormlike micellar solutions. Based on the two-species Vasquez–Cook–McKinley constitutive model for micelles, a recent numerical study shows that the breakage of long micelles downstream of the translating sphere causes this unsteady motion [C. Sasmal, "Unsteady motion past a sphere translating steadily in wormlike micellar solutions: A numerical analysis," J. Fluid Mech. **912**, A52, (2021)]. This numerical study further shows that the micelle breakage rate and wall slip can strongly influence this phenomenon. In particular, we find that the onset of this unsteady motion is delayed to higher values of the Weissenberg number as the micelle breakage rate decreases, or in other words, micelles become hard to break. Additionally, we observe that at some values of the micelle breakage rate, again, a transition in the flow field from unsteady to steady occurs at high Weissenberg numbers. Therefore, there is a window of the Weissenberg number present to observe this unsteady motion past the translating sphere. On the other hand, we show that the presence of wall slip on the sphere surface suppresses this unsteady motion past the translating

	sphere, and a probable explanation is also provided for the same.
24.	Effects of time-varying habitat connectivity on metacommunity persistence S Bhandary, D Biswas, T Banerjee, PS Dutta – Physical Review E, 2022 **Abstract:** Network structure or connectivity patterns are critical in determining collective dynamics among interacting species in ecosystems. Conventional research on species persistence in spatial populations has focused on static network structure, though most real network structures change in time, forming time-varying networks. This raises the question, in metacommunities, how does the pattern of synchrony vary with temporal evolution in the network structure. The synchronous dynamics among species are known to reduce metacommunity persistence. Here we consider a time-varying metacommunity small-world network consisting of a chaotic three-species food chain oscillator in each patch or node. The rate of change in the network connectivity is determined by the natural frequency or its subharmonics of the constituent oscillator to allow sufficient time for the evolution of species in between successive rewirings. We find that over a range of coupling strengths and rewiring periods, even higher rewiring probabilities drive a network from asynchrony towards synchrony. Moreover, in networks with a small rewiring period, an increase in average degree (more connected networks) pushes the asynchronous dynamics to synchrony. On the other hand, in networks with a low average degree, a higher rewiring period drives the synchronous dynamics to asynchrony resulting in increased species persistence. Our results also follow the calculation of synchronization time and are robust across other ecosystem models. Overall, our study opens the possibility of developing temporal connectivity strategies to increase species persistence in ecological networks.
25.	Evaluating environmental quality in Rujigou coalfield, China, using analytic hierarchy process V Saini, J Li, Y Yang, J Li - Environmental Science and Pollution Research, 2022 Abstract: Coal is the major fossil fuel used for power generation. Coal mining activities lead to environmental changes to a large extent, such as degradation in the quality of air, water, and soil, changes in landform, land use/land cover, and vegetation distribution. Evaluating the environmental quality is therefore essential to study the nature and impact of mining activities on the environment. The present study attempts to use the analytic hierarchy process (AHP) to assess the environmental quality of Rujigou coalfield that lacked previous such analysis. The criteria used for evaluation were selected through a literature review and extensive field survey. A photo tour of the study area shows the current ground conditions. Weights were assigned to these criteria based on expert opinions, recommendations from published literature, and field investigation. The results indicate that mining activities in the study region most significantly impact the air quality, followed by soil, water, landform, and vegetation. The knowledge of environmental quality can forewarn policymakers and mine managers about impending environmental problems and improve their ability to manage and resolve them. Moreover, the systematic methodological process described in this research can be applied to any study area with similar features to the one investigated in this paper.
26.	Existence of yttrium allotrope with incommensurate host–guest structure at moderate pressure: First evidence from computational approach P Tsuppayakorn-aek, T Bovornratanaraks, R Ahuja, T Bovornratanaraks, W Luo - Computational Materials Science, 2022

	Abstract: We predict an allotrope of yttrium with an incommensurate host–guest structure by using *ab initio* random structure searching technique, based on first-principles calculation. Along with this, we propose a set of analogous commensurate supercells, which is an incommensurate ratio (c_H/c_G), by approximating the different the number of guest atoms in channels in along c axis of the host structure. Herein, our results show that c_H/c_G = 5/4 is energetically stable. Subsequently, the incommensurate host–guest structure is found to be thermodynamically and dynamically stable within harmonic level. The hybridization of *spd* explains the stability of the host–guest structure under high pressure conditions. The distributions of electrons between the host and guest atoms indicate the strong and weak electron localizations of *spd* bonds. This findings suggest that the host–guest structure is more likely to be achieved experimentally in this metallic element at moderate pressure. **Graphical Abstract:** 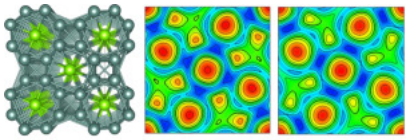 20 GPa 40 GPa
27.	Far from equilibrium transport on TASEP with pockets N Bhatia, AK Gupta - The European Physical Journal Plus, 2022 **Abstract:** We investigate a geometric adaptation of a totally asymmetric simple exclusion process with open boundary conditions, where each site of a one-dimensional channel is connected to a lateral space (pocket). The number of particles that may be accommodated in each pocket is determined by its capacity *q*. The continuum mean-field approximation is deployed for the case q=1q=1 where both lattice and pocket strictly follow the hard-core exclusion principle. In contrast, a probability mass function is utilized along with the mean-field theory to investigate the multiple-capacity case, where the pocket violates the hard-core exclusion principle. The effect of both finite and infinite reservoirs has been studied in the model. The explicit expression for particle density has been calculated, and the evolution of the phase diagram in α−βα−β parameter space obtained with respect to *q* and the attachment-detachment rates. In particular, the topology of the phase diagram is found to be unchanged in the neighborhood of q=1q=1. Moreover, the competition between lattice and pocket for finite resources and the unequal Langmuir kinetics captures a phenomenon in the form of a back-and-forth transition. We have also investigated the limiting case q→∞q→∞. The theoretically obtained phase boundaries and density profiles are validated through extensive Monte Carlo simulations.
28.	FASNet: Feature Aggregation and Sharing Network for Image Inpainting SS Phutke, S Murala - IEEE Signal Processing Letters, 2022 **Abstract:** Image inpainting is a reconstruction method, where a corrupted image consisting of holes is filled with the most relevant contents from the valid region of an image. To inpaint an image, we have proposed a lightweight cascaded architecture with *2.5 M parameters* consisting of encoder feature aggregation block (FAB) with decoder feature sharing (DFS) inpainting network followed by a refinement network. Initially, the FAB with DFS (inpainting) generator network is proposed which comprises of multi-level feature aggregation mechanism and feature sharing decoder. The FAB makes use of multi-scale spatial channel-wise attention to fuse

	weighted features from all the encoder levels. The DFS reconstructs the inpainted image with multi-scale and multi-receptive feature sharing in order to inpaint the image with smaller to larger hole regions effectively. Further, the refinement generator network is proposed for refining the inpainted image from the inpainting generator network. The effectiveness of proposed architecture is verified on CelebA-HQ, Paris Street View (PARIS_SV) and Places2 datasets corrupted using publicly available NVIDIA mask dataset. Extensive result analysis with detailed ablation study prove the robustness of the proposed architecture over state-of-the-art methods for image inpainting.
29.	Finite element analysis of heat assisted incremental sheet forming process N Kumar, A Agrawal, RM Belokar, N Kausshal - Advances in Materials and Processing Technologies, 2022 **Abstract:** Incremental sheet forming is a flexible method to produce 3D sculptured sheet metal parts without expensive and dedicated tools. The present work studies the behaviour of sheets with low ductility undergoing forming under warm conditions. The material selected is Ti6Al4 V titanium alloy which is very hard to deform at room temperature. The temperature of around 500 - 700°C, i.e. below the recrystallisation temperature, is provided to the sheet. In this numerical simulation, a predefined temperature of 500°C is provided initially to the sheet in the predefined field using ABAQUS® software to carry out the test runs. With the increase in temperature, the ductility of the material increases, and the sheet becomes easy to form. The analysis is carried out at a temperature range of 500 - 700°C with different process parameters, viz. step depth, wall angle, and constant tool diameter. Von-Mises stresses, forming depth, and thickness distribution at various input process parameters were studied in the present work. The results obtained show that the fracture depth and thickness distribution increase with a decrease in the mesh size and step depth, whereas they decrease with the decrease in the temperature and increase in the wall angle.
30.	Flow Dynamics in a Triple Swirl Burner N Vishnoi, A Valera-Medina, A Saurabh, L Kabiraj - Proceedings of the National Aerospace Propulsion Conference, Lecture Notes in Mechanical Engineering, 2022 **Abstract:** One of the most important milestones in gas turbine burner technology was the incorporation of swirling flows for flame stabilization. The objective of present work is the design and development of a generic fuel flexible multiple swirl burner with enhanced flashback resistance and low emissions. The burner design will allow operation in premixed and non-premixed modes with liquid and gaseous fuels. The investigated burner consists of 3 annular co-rotating swirlers: an outer radial swirler stage and two concentric axial swirler stages. Insights from the first isothermal and reactive numerical simulations for premixed methane–air combustion are being presented here. Results based on the characterization of the flow fields, temperature distribution, streamwise and azimuthal shear layer dynamics, and turbulence characteristics are presented. The velocity profiles obtained from isothermal numerical simulations are also validated by experimental results. Flame stabilization and flashback propensity are discussed with respect to the features of vortex breakdown, specifically the central recirculation zone (CRZ).
31.	Gold nanoparticles supported on ionic-liquid-functionalized cellulose (Au@CIL): A heterogeneous catalyst for the selective reduction of aromatic nitro compounds A Singh, N Singh, N Kaur, DO Jang - Applied Organometallic Chemistry, 2022

	Abstract: In response to the increasing need for green and cost-effective catalysts, a novel biomass-derived heterogeneous catalyst that is effective in a number of environmentally friendly applications has been synthesized. The heterogeneous catalyst (**Au@CIL**), composed of ionic-liquid-functionalized cellulose embedded with Au nanoparticles (NPs), was developed for the selective reduction of the nitro group. The Au NPs are formed by the reduction of Au^{3+} to Au^{0} with ascorbic acid while embedded in the solid support system. The presence of embedded Au NPs was confirmed using infrared spectroscopy, powder X-ray diffraction, scanning electron microscopy, zeta-potential measurements, energy-dispersive X-ray analysis, elemental dot mapping, and atomic force microscopy. In water at 30 °C, the heterogeneous catalyst **Au@CIL** selectively transforms aromatic nitro compounds into the corresponding amines in the presence of other functional groups, such as hydroxy, amino, aldehyde, carboxylic acid, and amide.
32.	High-power discrete vortex with phase locked lasers V Dev, V Pal - International Conference Laser Optics (ICLO), 2022 **Abstract:** We present the generation of high-power discrete vortices formed by phase locking one-dimensional ring array of lasers in a degenerate cavity. We have observed that the divergence of discrete vortices is independent of the topological charge, opposed to conventional continuous vortices. Further, we have found that discrete vortices exhibit good self-healing abilities against the obstructions in the source plane as well as propagated plane.
33.	High-Pressure Structural Transformation Pathway and Electronic Properties of $AgGaTe_2$: Ab Initio Evolutionary Structural Searching K Kotmool, P Tsuppayakorn-aek, W Luo, R Ahuja.. - The Journal of Physical Chemistry C, 2022 **Abstract:** We have used systematic ab initio evolutionary structural searching to uncover the high-pressure transformation pathway of a promising thermoelectric material, $AgGaTe_2$. The global structures of the ternary Ag–Ga–Te system have been predicted up to 100 GPa. The known chalcopyrite phase at ambient pressure is validated by the searching method. The B3-like structure with the space group (s.g.) of $P\bar{4}m_2$ exhibits a metastable one at a low-pressure range. The first structural phase transition is calculated at about 4 GPa, processing the $I\bar{4}_2d$ phase to a B1-like phase (s.g. *Pmma*). Other predicted structures, $Pmn2_1$ and *Pm* phases, are potentially coexisting phases up to 30 GPa because of the slightly different enthalpy. This finding reasonably explains the ambiguous results in the previous experiments. The high-pressure phase beyond 30 GPa is proposed to be a short-range alloy of bcc-Te and B2-AgGa rather than a cation-disordered B2-like phase. The band gap of the $I\bar{4}_2d$ phase is increased with increasing pressure, while the metastable $P\bar{4}m_2$ phase is a narrow band gap semiconductor. The electron–phonon coupling of the metallic phases of ternary IB-IIIA-VIA_2 compounds is derived for the first time in $AgGaTe_2$. They exhibit superconductors with a maximum T_c of 2.4 K in the *Pmma* phase at 6 GPa. The findings of this work not only provide a clear explanation of the high-pressure transformation pathway of $AgGaTe_2$ but also suggest promising electronic properties guiding further applications, especially in a thermometric device, of this material under high pressure.
34.	Integrating a covalent probe with ubiquicidin fragment enables effective bacterial infection imaging

	JB Mitra, S Chatterjee, A Kumar, A Bandyopadhyay.. - RSC Medicinal Chemistry, 2022 **Abstract:** Developing potent and novel bacterial imaging agents remains formidable due to the rapid development of bacterial resistance. Ubiquicidin and its derivatives are the most studied antimicrobial peptides that bind to anionic membranes of a broad range of bacterial pathogens. Studies reveal that UBI (29-41) labeled with ^{99m}Tc and ^{68}Ga could distinguish sterile inflammation from infection. A significant challenge that remains for cationic peptides is their poor salt tolerance. The present study deliberates the increment of UBI (29-41) peptide interaction with the bacterial membrane by incorporating 2-acetylphenylboronic acid (2-APBA) as a covalent probe and developing infection imaging probes with improved retention at the target. Given that both ^{99m}Tc-UBI (29-41) and ^{99m}Tc-UBI (29-41)-2-APBA peptide complexes are stable in serum over 16 h, ^{99m}Tc-UBI (29-41)-2-APBA shows enhanced uptake in *S. aureus* cells as compared to ^{99m}Tc-UBI (29-41). SPECT imaging in a mouse model of infection exhibited a higher target to non-target ratio after 2 h in the case of ^{99m}Tc-UBI (29-41)-2-APBA. The present study reveals a synergistic mechanism of target binding through covalent conjugation and non-covalent interaction, which could be a potential strategy for improving bacterial infection imaging. As a proof of concept, ^{99m}Tc-UBI (29-41)-2-APBA elicits our hypothesis by *in vivo* imaging of bacterial infection.
35.	Investigation on the sensitivity of indentation devices for detection of fatigue loading induced damage in bovine cortical bone P Uniyal, A Sharma, N Kumar - Journal of Biomechanics, 2022 **Abstract:** Daily physiological activities subject our skeletal system to cyclic loading with varying frequencies and magnitudes. These loadings interact with the microstructure of bone and create microdamage, which can cause stress-induced injuries if not repaired on the time. The early detection is required to prevent the complications associated with these fractures. In the present study, to examine fatigue loading-induced damage in cortical bone, the sensitivity of four different indentation devices was investigated. For this, cortical bone samples were fatigued in four-point bending configuration at 0.5 Hz, 2 Hz and 4 Hz frequencies. Following the fatigue loading, cyclic reference point indentation (cRPI), impact reference point indentation (iRPI), Vickers microhardness and nanoindentation tests were performed on the bone samples. Results show that indentation devices are sensitive to detect fatigue loading induced damage only in 0.5 Hz group samples on compressive region. On the other hand, the sensitivity of indentation devices for tensile stress-induced damage is not clear. Also, histological examination of fatigued bone samples shows a significant increase in the crack density and crack length with fatigue loading only for the 0.5 Hz group samples. The present study provides insight into the sensitivity of different indentation devices to fatigue loading induced damage, which could be helpful in the development of new devices for the early diagnosis of stress induced injuries.
36.	IPDCN2: Improvised Patch-based Deep CNN for facial retouching detection K Sharma, G Singh, P Goyal - Expert Systems with Applications, 2022 **Abstract:** With the advancement of photo editing softwares, nowadays facial retouching becomes a common practice across different social media platforms, Curriculum Vitae (CV) related websites, photo sharing applications, and magazines publishing flawless facial images of celebrities. In this paper, we propose an improvised patch-based deep convolution neural network (IPDCN2) to classify whether a facial image is original or retouched. The proposed

	network comprises of three stages i.e., pre-processing, high-level features extraction, and classification. Initially, we propose a pre-processing stage to extract only relevant patches from the input image by using 68 facial landmarks. In the second stage, an efficient and robust CNN based on residual learning is employed to extract the high-level hierarchical features from these patches. The proposed network uses the concept of residual learning with the help of max pooling layers to maximize the information flow across the neural network. Lastly, the extracted high-level features are passed to fully-connected layers for classification. The experimental results show that proposed network outperforms the existing state-of-the-art techniques by providing an accuracy of 99.84% on ND-IIITD dataset. Moreover, proposed network provides a classification accuracy of 95.80%, 83.70%, and 97.30% on YMU, VMU, and MIW make-up datasets, respectively.
37.	Metal-Free, Biomass-Derived Nano-Architectured Carbon Quantum Dots as an Efficient Acid-Base Bifunctional Catalyst for Facile Synthesis of Benzo[g]chromene and Pyrimidine Analogs A Singh, G Singh, S Sharma, N Kaur, N Singh - ChemistrySelect, 2022 **Abstract:** Herein, we have developed metal free, green, sulfonic acid functionalized carbon quantum dots-based an efficient acid-base bifunctional catalyst for green synthesis of benzo[g]chromene and pyrimidine analogs. The developed heterogenous catalyst exhibits significant reusability up to six cycles without any significant loss in its catalytic activity. Therefore, an economical and sustainable protocol has been developed for facile synthesis of biologically important heterocycles. Perusal of literature reports revealed that variedly functionalized carbon quantum dots (CQDs) have been extensively studied as sustainable alternative to conventional nanomaterials in catalysis. In this context, herein, we have designed and developed an efficient, metal free, green and heterogeneous sulfonic acid functionalized carbon quantum dots (CQDs)-based catalyst derived from biomass for one pot multicomponent reactions. The developed catalyst has been fully characterized using various techniques such as DLS, IR spectroscopy and zeta potential measurements. The synthesized catalyst acts as a bipolar catalyst which can activate all the three components via hydrogen bond donor as well as hydrogen bond acceptor sites in the reaction mixture, to synthesize pyrimidine and 4H-benzo[g]chromene derivatives in pure aqueous medium. Further, the catalyst exhibits significant reusability up to six cycles without any significant loss in its catalytic activity. Therefore, an economical and sustainable protocol has been developed for facile syntheses of biologically important heterocycles through an efficient and easily recoverable biomass derived catalyst in pure aqueous medium. Apparently, the developed strategy provides good eco-scale and E-factor values, which are acceptable according to green chemistry protocols. 
38.	Microstructural and tribological properties of laser-treated cold-sprayed titanium/baghdadite deposits A Kumar, R Kant, H Singh - Journal of Materials Research, 2022

	Abstract: This work presents the laser-remelting effect on microstructure, microhardness, and wear properties of the baghdadite reinforced cold-sprayed titanium composite coatings for orthopedic implant applications. The obtained results of laser-remelted coatings are compared to the as-sprayed coatings. The process parameters for laser treatment of cold-sprayed coatings are verified experimentally using scanning electron microscopy (SEM) and a thermal imaging camera. The laser-treated coatings are analyzed with SEM and energy-dispersive spectroscopy (EDS). Furthermore, sliding wear analysis of the laser-treated and as-sprayed coatings is done in Hank's solution. The results show that laser-remelting helped in improving the density, microhardness, and wear resistance of the coatings. Post-wear analysis revealed that the main wear mechanism for coating wear is three-body abrasion and adhesion. **Graphical Abstract:** 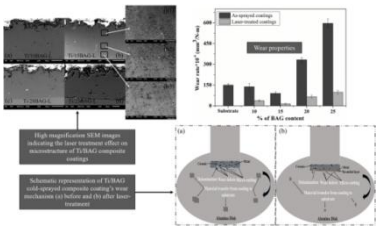
39.	New *ab initio* calculations and collisional properties of closed-shell NCCP ($^1\Sigma^+$) by collisions with He (^1S) TJ Dhilip Kumar - Monthly Notices of the Royal Astronomical Society, 2022 **Abstract:** NCCP, a phosphorous species, is believed to have been discovered in the carbon-rich star IRC+10216. Understanding collisional properties, such as cross-sections ($\sigma j \rightarrow j' \sigma j \rightarrow j'$) and rate coefficients ($kj \rightarrow j' kj \rightarrow j'$), is important for the reliable determination of molecular abundance. The non-reactive collisions between NCCP and He species at low temperatures are the subject of this study. Calculations are based on new *ab initio* potential energy surface (PES) of NCCP–He. The PES calculations are carried out at the CCSD(T)–F12a in conjunction with the aug-cc-pVTZ basis set. The PES is found to have a global minimum towards the N end with a well depth of -46.40 cm^{-1}. The *ab initio* points are analytically fitted on to the Legendre polynomial relevant for quantum scattering. From this fitted PES, the integral inelastic rotational cross-sections of NCCP with He collisions are computed for total energies up to 550 cm^{-1}, using the accurate close coupling approach of quantum mechanics. The resonances are observed at low total energies due to quasi-bound states of the NCCP−He complex. Rate coefficients are determined among the 19 lowest rotational levels of NCCP by thermally averaging the cross-sections at low temperatures. The de-excitation rate coefficients increase with decreasing Δj.
40.	Ni@4H-chromene-based core–shell nanoparticles: highly sensitive and selective chemosensors for the radiosensitizer bromodeoxyuridine G Bhardwaj, R Kaur, S Saini, N Kaur, N Singh – Journal of Materials Chemistry C, 2022 **Abstract:** Regardless of the significant use of 5-bromo-2′-deoxyuridine (BrdU) as a radiosensitizer and diagnostic tool in cancer patients, some severe side effects and health issues have been reported, such as genetic mutations, birth defects, and other inheritable genetic effects. Thus, it has become more important to quantify the amount of BrdU during its usage. With

	reference to this, Ni@4*H*-chromene (**Ni@G1**)-based core–shell nanoparticles have been fabricated and these show a great response for the selective and sensitive detection of BrdU. The formed **Ni@G1** exhibits no significant response with interfering thymidine analogs like iododeoxyuridine (EI) and ethynyl deoxyuridine (EdU) in competitive binding studies. **Ni@G1** shows the ability to sense BrdU up to a detection limit of 9 nM and no significant interference is shown by pH, salt and temperature. A comparison of studies in aqueous and organic media further reveals that the sensor reported here shows an excellent response in an aqueous medium. 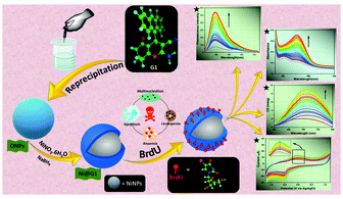
41.	Non-conserving exclusion process with a dynamic obstacle B Pal, AK Gupta - Chaos, Solitons & Fractals, 2022 **Abstract:** Motivated by complex transport processes occurring in biological and physical systems, we study a non-conserving totally asymmetric simple exclusion process with a dynamic defect particle. The defect particle may appear or disappear stochastically and slows down the traffic of moving particles while bound to the lattice. We analyze the system in the context of mean-field approach, and investigate the steady state properties which exhibit a rich dynamic behavior. The theoretically obtained density profiles and current fully describe the phase diagram, further allowing to elucidate the effect of various dynamics individually. Depending upon non-conserving kinetics and defect dynamics, phase schema displays at most eighteen phases; in total, the system exhibits twenty-one phases. Several critical values of the kinetic rates that trigger a qualitative change in the phase diagrams are obtained using analytical arguments. The theoretical outcomes are validated through extensive Monte Carlo simulations.
42.	Novel use of ultrasonic-assisted turning in conjunction with cryogenic and lubrication techniques to analyze the machinability of Inconel 718 J Airao, CK Nirala, N Khanna - Journal of Manufacturing Processes, 2022 **Abstract:** Industries have been pursuing a competent machining system that meets the necessity of sustainability without deteriorating tool wear or final part quality of components made from difficult-to-cut material ‘Inconel 718’. In this regard, a novel study, applying ultrasonic vibration along with lubrication (MQL) and cooling (LCO_2) is proposed to enhance the machinability of Inconel 718. The purpose of this work is to examine the machinability of Inconel 718 in conventional and ultrasonic-assisted turning (UAT) under dry, wet, MQL, and LCO_2. The experiments are performed on an in-house developed UAT setup, keeping all the machining parameters constant. The LCO_2 considerably reduces edge chipping, nose wear, adhesion, and abrasion wear in both the processes. Quantitatively, the conventional turning under LCO_2 reduces the flank wear by 32–60 %, power consumption by 4–41 %, and power consumption by 5–31 % compared to dry, wet, and MQL strategies. Similarly, the UAT under LCO_2 reduces the flank wear by 32–53 %, power consumption by 11–40 % and power consumption by 5–31 % compared to dry, wet, and MQL strategies. The UAT reduces the

	surface roughness and power consumption compared to conventional turning when used under MQL and LCO_2. The LCO_2 in conjunction with ultrasonic vibration significantly reduces specific cutting energy and tool wear without compromising the surface quality. Moreover, the combination also helps in enhancing the chip breakability and reducing the strain localization. Ultimately, the UAT, along with LCO_2 promotes sustainability in the machining of Inconel 718.
43.	Numerical investigations on the difference between aiding and opposing flows in the developing regime of laminar mixed convection in vertical tubes S Gorai, SK Das, D Samanta - Numerical Heat Transfer, Part A: Applications, 2022 **Abstract:** The present article discusses the numerical simulation results of laminar mixed convection flow in vertical tubes. A comparative analysis of the thermal and hydrodynamic features of both buoyancy-assisted and opposed flows was performed for Reynolds number ($100 \le Re \le 2300100 \le Re \le 2300$), Grashof number ($10^3 \le Gr \le 7.935\times106103 \le Gr \le 7.935\times10^6$) and Richardson number ($0.1 \le Ri \le 1.50.1 \le Ri \le 1.5$) with uniform heat flux boundary condition. 2-D axisymmetric steady state simulations were carried out for a length-to-diameter (L/DL/D) ratio of $\le 1000\le 1000$ with water as the working fluid. Numerical simulations were performed by employing SIMPLE scheme for pressure–velocity coupling in momentum equations and second order UPWIND scheme for solving energy equations. In case of assisting flow (Re∼250Re∼250), at fully developed state the centerline velocity decreases, and velocity is increased near the tube wall due to heat flux induced free convection. With increasing heat flux, the decrement in centerline velocity compared to the no-heat flux condition increases. Further, with increasing heat flux, the increase in friction factor and Nusselt number was observed. Therefore, at the same Re,Re, the variation of heat flux led to unique velocity profiles and temperature gradients. The variation of centerline velocity and temperature in developing region was also studied. While centerline temperature was monotonically increasing with length, the centerline velocity increased up to a maximum in the developing region and then attained the steady state at a lower value in the fully developed state. Subsequently we studied the dependence of RiRi on the hydrodynamic and thermal features. For constant Re,Re, friction factor and Nusselt number was observed to increase with increase in RiRi from 0.1 to 1.5 range. At fixed Re,Re, variation of heat flux leads to variation of GrGr or Ri.Ri. Hence, the buoyancy effect has a significant role in the entrance length development. The hydrodynamic entry length after an initial increase, attained an almost constant value with increasing Ri.Ri. On the other hand, the thermal entry length exhibited a decreasing trend with increasing Ri.Ri. Similarly, at constant Ri,Ri, Nusselt number increased with increasing ReRe for a range of 100–1000. It was evident that for a given ReRe and Ri,Ri, the heat transfer in the developing flow is always higher as that of the fully developed flow. Contrasting observations were observed for buoyancy-opposed flow. Velocity is accelerated at the center as compared to the tube wall in case of opposing flow for same ReRe and Ri.Ri. For a fixed Re,Re, the friction factor and Nusselt number decreased with increasing the Ri.Ri. Both the hydrodynamic and thermal entry length increases for opposing flows. Finally, we have developed correlations for fully developed friction factor (ff) with ReRe as well as RiRi and Nusselt number (NuNu) with RiRi for buoyancy-assisting and buoyancy-opposing flows. Two independent correlations are also produced for NuNu with Graetz number (GzGz) for developing and fully developed regimes in both assisting as well as opposing flows.

44.	Numerical Modelling of Conical-Shaped Bone Marrow Biopsy Needle Into Multilayer Iliac Crest Model R Nadda, R Repaka, A Sahani - Journal of Engineering and Science in Medical Diagnostics and Therapy, 2022 **Abstract:** Bone marrow biopsy (BMB) is a standard technique used in various therapies, research, diagnosis, and prognosis. The extensive forces during biopsy result in unnecessary stress concentrations that are primarily hazardous to weak end bones. To enhance protection and to better identify the risks of bone biopsy, it is essential to understand and predict the interaction of needles with multiple layers of skin and bone. The present investigation aimed to find out the numerical evaluation of forces involved in the insertion and extraction of the needle into multilayer iliac crest model. The insertion and extraction forces have been studied at different diameters of biopsy needles up to a depth of 15.35 mm and insertion speeds in the range of 1 mm/sec - 10 mm/sec. The results showed that the insertion and extraction forces vary according to the needle diameter and relative velocity among the needle and tissue layers. A linear force vs. depth relationship has been obtained in the preliminary phase, and as the depth of insertion increases, the forces increase non-linearly. At the end phase of penetration, the forces augmented more rapidly at a low insertion rate compared to the high insertion rate.
45.	Oxygen Vacancy-Mediated *Z*-Scheme Charge Transfer in a 2D/1D B-Doped g-C_3N_4/rGO/TiO_2 Heterojunction Visible Light-Driven Photocatalyst for Simultaneous/Efficient Oxygen Reduction Reaction and Alcohol Oxidation A Behera, AK Kar, R Srivastava - Inorganic Chemistry, 2022 **Abstract:** Hydrogen peroxide (H_2O_2) is a powerful oxidant that directly or indirectly oxidizes many organic and inorganic contaminants. The photocatalytic generation of H_2O_2 is achieved by using a semiconductor photocatalyst in the presence of alcohol as a proton source. Herein, we have synthesized oxygen vacancy (O_v)-mediated TiO_2/B-doped g-C_3N_4/rGO (TBCN@rGO) ternary heterostructures by a simple hydrothermal technique. Several characterization techniques were employed to explore the existence of oxygen vacancies in the crystal structure and investigate their impact on the optoelectronic properties of the catalyst. Oxygen vacancies offered additional sites for adsorbing molecular oxygen, activating alcohols, and facilitating electron migration from TBCN@rGO to the surface-adsorbed O_2. The defect creation (oxygen vacancy) and *Z*-scheme mechanistic pathways create a suitable platform for generating H_2O_2 by two-electron reduction processes. The optimized catalyst showed the highest photocatalytic H_2O_2 evolution rate of 172 μmol/h, which is 1.9 and 2.5 times greater than that of TBCN and BCN, respectively. The photocatalytic oxidation of various lignocellulose-derived alcohols (such as furfural alcohol and vanillyl alcohol) and benzyl alcohol was also achieved. Photocatalytic activity data, physicochemical and optoelectronic features, and trapping experiments were conducted to elucidate the structure–activity relationships. The TBCN@rGO acts as a multifunctional *Z*-scheme photocatalyst having an oxygen vacancy, modulates surface acidity–basicity required for the adsorption and activation of the reactant molecules, and displays excellent photocatalytic performance due to the formation of a large number of active surface sites, increased electrical conductivity, improved charge transfer properties, outstanding photostability, and reusability. The present study establishes a unique strategy for improving H_2O_2 generation and alcohol oxidation activity and also provides insights into the significance of a surface vacancy in the semiconductor photocatalyst.

	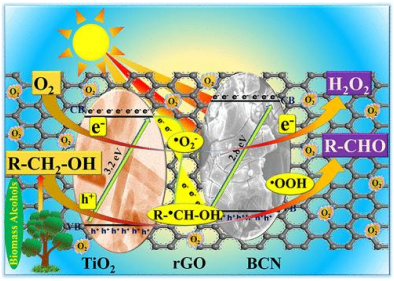
46.	Peculiarities of Seismic Risk in Hilly Regions: Topographic Effects on Hazard and Vulnerability D Lang, Y Singh, S Molina, M Surana - European Conference on Earthquake Engineering and Seismology, Progresses in European Earthquake Engineering and Seismology, 2022 **Abstract:** Many of the world's high-seismic hazard regions are characterized by hilly topography. Topographical features pose significant problems when it comes to the seismic safety of buildings and infrastructure facilities, both with respect to the seismic impact, the structure's vulnerability and potential secondary hazards such as slope stability-related issues. The seismic ground motion characteristics are greatly influenced by the geometry of topographical features such as slopes, hilltops, ridges and canyons and their relationship with the geologic materials partly overlying these features. Both, topography and geology lead in most cases to a significant amplification of the seismic ground motion and hence increased seismic demand to buildings located in these areas. This comes in addition to the fact that buildings located in hilly areas have a significantly lower structural capacity. Due to the limitations posed by the hill topography and the scarcity of flat building plots, many buildings are placed on hill slopes thus have highly irregular configurations, both in plan and elevation, making them highly vulnerable to seismic impact. The manuscript focuses on selected case studies in the Indian Himalayas, which are not only the youngest mountains, but also one of the most seismic areas in the world. Influence of topography on seismic hazard and vulnerability of buildings in the study area is illustrated using extensive numerical studies. The gross effect of these two parameters is demonstrated by comparing the probabilistic earthquake loss estimates with and without considering the topographic effects.
47.	Performance Analysis of Evaporation and Heat Wheel-Based Building Air Conditioning Systems G Singh, R Das - Journal of Energy Resources Technology, 2022 **Abstract:** Air-conditioning in composite weather is relatively more challenging and also carries importance as it resembles conditions of hot-dry, cold, and warm-humid climates. Bifurcation of cooling and ventilation tasks happens to be one of the attractive techniques to design energy efficient air-conditioning systems. It deals with the concept of providing a dedicated outdoor air system (DOAS) in conjunction with the air-conditioning unit. This study establishes electrical energy consumption behaviour of a building air-conditioning unit when modifications are done along the air pathway of the desiccant-integrated DOAS. For a 511 m^2 building situated in composite weather, simulations in EnergyPlus are carried out after necessary validations with the available standards. Here, two modes are discussed, in the first one, an indirect evaporation cooler (IEC) based system is analysed, while in the second mode, a heat wheel has been studied. For regeneration, a solar collector and supplementary electrical heater are provided. For dynamic

	pattern of site environmental conditions, variations of room air temperature, humidity, thermal load, electricity, thermal energy, and solar fraction have been studied. Current analysis demonstrates that approximately 2994 kWh of the total thermal energy delivered by solar collector and supplementary electrical heater system can be saved through heat wheel instead of IEC. The usage of a heat wheel in the air flow pathway of the desiccant-integrated DOAS can offer energy savings up to 5.04 % of the electrical energy with respect to IEC-integrated DOAS. Furthermore, the suggested design delivers higher solar fraction.
48.	Rational design of Cu(I)-anchored porous covalent triazine framework (CTF) for simultaneous capture and conversion of CO_2 at ambient conditions G Singh, CM Nagaraja - Journal of CO2 Utilization, 2022 **Abstract:** The selective carbon capture and utilization (CCU) as a C1 source is sought to be an important step towards environmental remediation and sustainable production of useful chemicals. In this context, herein, we report the strategic integration of noble metal-free Cu(I) catalytic sites with a nitrogen-rich, CO_2-philic, bipyridine functionalized covalent triazine framework (bipy-CTF) by a post-synthetic approach. The Cu(I)@bipy-CTF showed very good performance for simultaneous capture and fixation of CO_2 into α-alkylidene cyclic carbonates (α-aCCs), high-value commodity chemicals at ambient conditions. Further, the Cu(I) anchored bipy-CTF showed high CO_2 affinity with the interaction energy of 44.09 kJ/mol attributed to the presence of CO_2-philic, basic nitrogen sites. The presence of both CO_2-philic nitrogen and alkynophilic Cu(I) sites decorated in the 1D channels of bipy-CTF provided a good catalytic activity for the chemical fixation of carbon dioxide from dilute gas (13 % CO_2) to yield α-aCCs at atmospheric pressure (balloon) of CO_2. Notably, Cu(I)@bipy-CTF showed high recyclability and chemical stability for multiple catalytic cycles. Overall, the present work represents a rare example of a COF-based recyclable catalyst for CO_2 fixation from dilute gas into valuable chemicals under mild conditions.
49.	Regulating complex fluid sessile droplet evaporation kinetics by suppression of internal electro-convection A Kaushal, V Mehandia, P Dhar - Colloids and Surfaces A: Physicochemical and Engineering Aspects, 2022 **Abstract:** We report the phenomenology of suppression of the evaporation kinetics of electrically conducting saline sessile droplets in the presence of transverse electric field stimulus. Our experimental results show that the evaporation rates (on hydrophilic and superhydrophobic surfaces) of saline droplets are higher than water droplets, but the rates reduce when an alternating electric field is applied across the saline droplets. The reduction is noted to be a direct function of the electric field strength, and the contact line dynamics of the drying droplet are largely affected. After the classical vapour-diffusion-driven evaporation models fail to explain the modified evaporation kinetics, the flow visualization and infrared thermography were performed to diagnose the internal thermo- and solutal-electrohydrodynamics. Suppression of the internal circulation velocities is observed in the saline sessile droplets under the application of the electric field. A scaling analysis model is proposed based on the internal advection mechanisms to quantify the role of electrohydrodynamics, electro-thermal, electro-solutal convection, and the Electrohydrodynamic number on the internal circulation velocity and evaporation rates. The model incorporates the effects played by the governing Marangoni, Capillary, evaporative Jacob, electro-Prandtl, and electro-Schmidt

	numbers towards morphing the thermo-solutal advection and is in agreement with the experimental results. An interfacial shear modified Stefan flow analysis is put forward to determine the reduced evaporation rates, and a good match with the experimental observations is obtained.
50.	Scheduling algorithms for truly heterogeneous hierarchical fog networks A Kaur, N Auluck - Software: Practice and Experience, 2022 **Abstract:** Fog computing has emerged as a viable framework for processing delay sensitive applications. Modern applications consist of latency-sensitive and latency-tolerant jobs, leading to fog architectures that are often multi-tiered/hierarchical. *FiFSA* (hierarchical first fog scheduling algorithm) and *EFSA* (hierarchical elected fog scheduling algorithm) are capable of scheduling both online and batch jobs on hierarchical fog-cloud architectures. We consider heterogeneity in computing capacity—both among fog devices in separate layers, and among fog devices in the same layers. In general, online jobs with modest cpu requirements are scheduled on lower tier fog devices, and batch jobs with significant cpu requirements are scheduled on higher tier-fog nodes, or the cloud data center (*cdc*). *FiFSA* assigns jobs to the first fog device with sufficient spare capacity. *EFSA* employs a MinMin heuristic that assigns jobs to the fog device that results in minimum completion time, while considering fog load. The performance of the proposed algorithms has been evaluated on a real-life workload trace, using both simulation scenarios and a prototype testbed. *FiFSA* and *EFSA* offer an improvement of 19% to 70% in completion times and an improvement of 42% to 72% in system cost over other comparable algorithms.
51.	Self-Supervised Approach for Facial Movement Based Optical Flow M Alkaddour, U Tariq, A Dhall - IEEE Transactions on Affective Computing, 2022 **Abstract:** Computing optical flow is a fundamental problem in computer vision. However, deep learning-based optical flow techniques do not perform well for non-rigid movements such as those found in faces, primarily due to lack of the training data representing the fine facial motion. We hypothesize that learning optical flow on face motion data will improve the quality of predicted flow on faces. This work aims to: (1) exploring self-supervised techniques to generate optical flow ground truth for face images; (2) computing baseline results on the effects of using face data to train Convolutional Neural Networks (CNN) for predicting optical flow; and (3) using the learned optical flow in micro-expression recognition to demonstrate its effectiveness. We generate optical flow ground truth using facial key-points in the BP4D-Spontaneous dataset. This optical flow is used to train the FlowNetS architecture to test its performance on the Extended Cohn-Kanade dataset and a portion of the generated dataset. The performance of FlowNetS trained on face images surpassed that of other optical flow CNN architectures. Our optical flow features are further compared with other methods using the STSTNet micro-expression classifier, and the results indicate that the optical flow obtained using this work has promising applications in facial expression analysis.
52.	Sheet Atomization of Gel Propellant Simulant K Vivek, A Saurabh, D Deshmukh, D Agarwal, L Kabiraj - Proceedings of the National Aerospace Propulsion Conference, Lecture Notes in Mechanical Engineering, 2022 **Abstract:** Gelled propellants for rocket propulsion applications offer the advantage of safer storage and handling in comparison with liquid fuels. Sheet formation and break-up study of

	non-reactive gel simulant prepared with Carbopol 934 in de-ionized water was conducted for understanding atomization of gels by impinging jets configuration. Material properties of gels prepared and their flow behavior estimated. The simulant is injected through an orifice of 0.413 mm up to a range of 20 bar injection pressure is studied by analyzing high-speed shadow graph images of liquid jets impingement, sheet formation, and disintegration. The prominent effect of gelling agent concentration in sheet formation and break-up is revealed. Sheet break-up is occurring in two different modes for five different gel concentrations. Waves generated from impingement point caused break-up of sheets for low-concentration gels and high-velocity jets while tearing and hole formation in sheets led to their break-up for mostly high-concentration gels and particularly for low jet velocity modes. Droplet trajectories and their velocity at various locations in the periphery of sheets were measured for two different jet velocities for five gel concentrations.
53.	Strategic Design of Mg-Centered Porphyrin Metal–Organic Framework for Efficient Visible Light-Promoted Fixation of CO_2 under Ambient Conditions: Combined Experimental and Theoretical Investigation R Das, SS Manna, B Pathak, CM Nagaraja - ACS Applied Materials & Interfaces, 2022 **Abstract:** The sunlight-driven fixation of CO_2 into valuable chemicals constitutes a promising approach toward environmental remediation and energy sustainability over traditional thermal-driven fixation. Consequently, in this article, we report a strategic design and utilization of Mg-centered porphyrin-based metal–organic framework (MOFs) having relevance to chlorophyll in green plants as a visible light-promoted highly recyclable catalyst for the effective fixation of CO_2 into value-added cyclic carbonates under ambient conditions. Indeed, the Mg-centered porphyrin MOF showed good CO_2 capture ability with a high heat of adsorption (44.5 kJ/mol) and superior catalytic activity under visible light irradiation in comparison to thermal-driven conditions. The excellent light-promoted catalytic activity of Mg–porphyrin MOF has been attributed to facile ligand-to-metal charge transfer transition from the photoexcited Mg–porphyrin unit (SBU) to the Zr_6 cluster which in turn activates CO_2, thereby lowering the activation barrier for its cycloaddition with epoxides. The in-depth theoretical studies further unveiled the detailed mechanistic path of the light-promoted conversion of CO_2 into high-value cyclic carbonates. This study represents a rare demonstration of sunlight-promoted sustainable fixation of CO_2, a greenhouse gas into value-added chemicals.
54.	Strong Optical Excitation and High Thermoelectric Performance in 2D Holey-Phosphorene Monolayer N Khossossi, Deobrat Singh, Wei Luo, R Ahuja – Energy Technology, 2022 **Abstract:** Through density functional theory (DFT)-based computations, a systematic exploration of the newly predicted 2D phosphorene allotrope, namely holey-phosphorene (HP), is carried out. It is revealed that HP shows a semiconducting nature with an indirect bandgap of 0.83 eV upon Perdew-Burke-Ernzerhof (PBE) functional. Then, to survey the optical features, a (G_0W_0)-based approach is employed to solve the Bethe–Salpeter equation to derive the intra-layer excitonic effects. It is derived via the absorption spectrum, that HP presents an excitonic binding strength of 1.47/1.96 eV along the *x*/*y*-direction with the first peak of the absorption at 0.92/0.43 eV for the *x*/*y*-direction. The thermoelectric properties are also explored in detail and reveal a very high thermal power value along with an enhanced figure of merit (ZT) of about 3.6. The 2D HP monolayer for thermoelectric performance has high thermoelectric conversion

	efficiency (TCE) and is estimated to be about 22%. All these outstanding findings may be attributed to the quantum confinement effect of the porous geometry of the 2D HP nanosheet, thereby confirming its relevance as a prospect for high-performance optoelectronic and thermoelectric engineering systems.
55.	Study of the Incomplete Fusion reaction dynamics for the system 14N + 169Tm using the Forward Recoil Range Distribution technique S Kumar, PK Giri, R Kumar, A Yadav, R Ali, A Babu, ..PP Singh.. - Journal of Physics G: Nuclear and Particle Physics, 2022 **Abstract:** Studies in the past have demonstrated that complete fusion and incomplete fusion dynamics are both significant just above the Coulomb barrier, yet the dynamics of incomplete fusion are elusive since they are so complex below 10 MeV/nucleon. In order to investigate low-energy incomplete fusion dynamics, we measured the forward recoil range distribution of evaporation residues populated in the system 14N + 169Tm at energy ≈ 5.9 MeV/nucleon. A stack target-catcher activation technique followed by offline-γ- spectroscopy was used to estimate the forward recoil range distribution of the evaporation residues. In order to investigate a new parameter for describing incomplete fusion dynamics, the incomplete fusion fraction (FICF (%)) for the present system was estimated from the range-integrated cross-sections and compared with other systems in the literature. The forward recoil range distribution and range integrated cross-sections of seven evaporation residues have been estimated experimentally. These cross-section results agree well with the experimental results obtained from the excitation functions. On re-investigation of entrance channel systematics for Qα value of projectile, mass-asymmetry (μMA), and Coulomb factor (ZP ZT), it has been found that the Qα-value systematic for 14N is not valid at all projectile energies. The forward recoil range distribution measurement is one of the direct methods available to probe the complete and incomplete fusion contributions in evaporation residues at low projectile energy. It has also been observed that the dynamics of ICF are not only dependent on the parameters of one entrance channel but on multiple entrance channels. We have also introduced the entrance channel parameter Zeta (ζ) for the first time in Incomplete Fusion reactions to see the combined effect of mass-asymmetry (μMA) and ZP ZT, as this parameter is better suited than μMA and ZP ZT individually and has a linear dependency on FICF (%).
56.	Superconducting Gap of Pressure Stabilized $(Al_{0.5}Zr_{0.5})H_3$ from *Ab Initio* Anisotropic Migdal–Eliashberg Theory P Tsuppayakorn-aek, R Ahuja, T Bovornratanaraks.. – ACM Omega, 2022 **Abstract:** Motivated by Matthias' sixth rule for finding new superconducting materials in a cubic symmetry, we report the cluster expansion calculations, based on the density functional theory, of the superconducting properties of $Al_{0.5}Zr_{0.5}H_3$. The $Al_{0.5}Zr_{0.5}H_3$ structure is thermodynamically and dynamically stable up to at least 200 GPa. The structural properties suggest that the $Al_{0.5}Zr_{0.5}H_3$ structure is a metallic. We calculate a superconducting transition temperature using the Allen–Dynes modified McMillan equation and anisotropic Migdal–Eliashberg equation. As result of this, the anisotropic Migdal–Eliashberg equation demonstrated that it exhibits superconductivity under high pressure with relatively high-T_c of 55.3 K at a pressure of 100 GPa among a family of simple cubic structures. Therefore, these findings suggest that superconductivity could be observed experimentally in $Al_{0.5}Zr_{0.5}H_3$.

	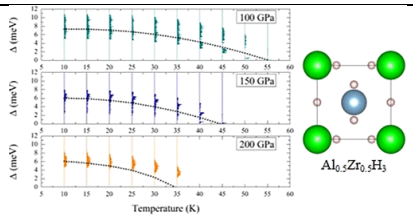
57.	System Parameter Identification of a Colored-Noise-Driven Rijke Tube Simulator N Vishnoi, V Gupta, A Saurabh, L Kabiraj - Journal of Engineering for Gas Turbines and Power, 2022 **Abstract:** In this paper, we report an experimental investigation on the influence of colored noise (generated by the Ornstein–Uhlenbeck (OU) process) on thermoacoustic coupling in an electro-acoustic Rijke tube simulator. In the absence of noise, the simulator exhibits subcritical Hopf bifurcation. Although noise in a practical system has a finite correlation time, yet the system identification methods are based on the assumption of white noise. In this study, we investigate the effects of correlation time, and intensity of colored noise on the estimation of the growth rates of acoustic oscillations determined using Fokker–Planck equation in stable, bistable, and linearly unstable regions. Subsequently, we compare the findings against results obtained considering white noise approximations. We report the observed deviation of the estimated growth rates from the actual values as a function of noise intensity and correlation time. We find that with the colored noise model, the deviation in the estimated growth rates lies within the range of 0–10% compared to the deviation of 5–25% observed considering the white noise approximation. We also report that increasing noise amplitudes leads up to a deviation of approximately 30% in the estimated growth rates from the actual values.
58.	Tool wear reduction in machining Inconel 718 by using novel sustainable cryo-lubrication techniques J Airao, N Khanna, CK Nirala - Tribology International, 2022 **Abstract:** Combining different cooling and lubrication strategies to reduce the tool wear and enhance the machinability of Inconel 718 is a new approach to be studied. In this regard, the present article uses two different cooling strategies to increase the machinability of Inconel 718. Six different approaches of cooling strategies, i.e., Cryo-MQL (*LCO_2 delivers on rake* and *MQL on Flank*), MQL- Cryo, EMQL- Cryo, Cryo -EMQL, EMQL-MQL and MQL-EMQL are used for experiments. The tool wear, specific cutting energy, power consumption, surface roughness, and chip morphology are inspected. The flow of LCO_2 on the rake face and the EMQL on the flank face considerably reduce the tool wear, surface roughness, power and specific cutting energy consumption, in comparison to other strategies. This novel combination of LCO_2 and EMQL improves sustainability without compromising surface quality in machining Inconel 718.
59.	Tuning the selective sensing properties of transition metal dichalcogenides (MoX_2: X= Se, Te) toward sulfurrich gases P Panigrahi, Y Pal, D Raval, ..R Ahuja.. - Materials Today Chemistry, 2022 **Abstract:** There is an urgent need for an efficient sensor to mitigate the effects of toxic pollutants possessing severe impacts on humans and the environment. Motivated by this, we investigated the selected transition metal dichalcogenides (MoX_2: X = Se, Te) monolayers

	toward the toxic sulfur-containing gases, such as H_2S and SO_2. We employed density functional theory simulations in combination with nonequilibrium Green's function formalism to study the optimized geometries, binding strength, electronic structures, charge transfer mechanism, and transport (current–voltage) characteristics of MoX_2 with and without H_2S and SO_2. Weak binding energies (<-0.30 eV) of H_2S/SO_2 on pristine MoX_2 were enhanced by selectively substituting the latter with elements like As, Ge, and Sb at lower doping concentrations of around 2%. We find that the doped MoX_2 strongly adsorbs H_2S/SO_2 yielding significant changes in their electronic properties, which were the fundamentals for the efficient sensing mechanism and were studied through the density of states and work function calculations. For the practical sensing applications, we considered the statistical thermodynamic analysis to investigate the sensing properties of pristine and doped MoX_2 monolayers under varied conditions of the temperatures and pressures. We are confident that our findings would pave the way for synthesizing sensitive and selective transition metal dichalcogenides-based nanosensor toward H_2S/SO_2.
60.	Ultrathin Durable Organic Hydrophobic Coatings Enhancing Dropwise Condensation Heat Transfer A Tripathy, K Regulagadda, CWE Lam, MA Donati, CS Sharma.. - Langmuir, 2022 **Abstract:** Organic hydrophobic layers targeting sustained dropwise condensation are highly desirable but suffer from poor chemical and mechanical stability, combined with low thermal conductivity. The requirement of such layers to remain ultrathin to minimize their inherent thermal resistance competes against durability considerations. Here, we investigate the long-term durability and enhanced heat-transfer performance of perfluorodecanethiol (PFDT) coatings compared to alternative organic coatings, namely, perfluorodecyltriethoxysilane (PFDTS) and perfluorodecyl acrylate (PFDA), the latter fabricated with initiated chemical vapor deposition (iCVD), in condensation heat transfer and under the challenging operating conditions of intense flow (up to 9 m s–1) of superheated steam (111 °C) at high pressures (1.42 bar). We find that the thiol coating clearly outperforms the silane coating in terms of both heat transfer and durability. In addition, despite being only a monolayer, it clearly also outperforms the iCVD-fabricated PFDA coating in terms of durability. Remarkably, the thiol layer exhibited dropwise condensation for at least 63 h (>2× times more than the PFDA coating, which survived for 30 h), without any visible deterioration, showcasing its hydrolytic stability. The cost of thiol functionalization per area was also the lowest as compared to all of the other surface hydrophobic treatments used in this study, thus making it the most efficient option for practical applications on copper substrates. 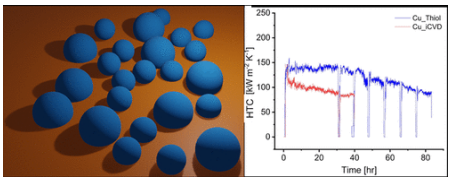

Disclaimer: This publication digest may not contain all the papers published. Library has compiled the publication data as per the alerts received from Scopus and Google Scholar for the affiliation "Indian Institute of Technology Ropar" for the month of August 2022. The author(s) are requested to share their missing paper(s) details if any, for the inclusion in the next publication digest.